Simulation of Thermal Contraction Strain Correction to g-Factor in Quantum Dot Qubit Device

Luca Niu
Department of Physics and Astronomy, University of California, Los Angeles
(Dated: June 23, 2024)

The g-factor is pivotal for controlling quantum dot qubits, as it directly influences the Hamiltonian dynamics. In quantum dots, strain can adjust the g-factor by modulating the energy gap between the heavy hole (HH) and light hole (LH) bands in Germanium. The strain is represented by a 3×3 tensor whose distribution within the device can be complex, largely due to thermal contraction effects. This paper utilizes the Finite Element Method (FEM) to simulate this strain and the resultant corrections to the g-factor by solving the derived equations for thermal expansion. Our findings indicate that the corrections to the in-plane components of the g-factor are on the order of $10^{-2}\mathrm{V}^{-1}$, while the out-of-plane components are approximately $10^{-1}\mathrm{V}^{-1}$. These substantial corrections not only deepen our understanding of strain effects in quantum dot devices but also lay the groundwork for precise g-factor tuning to enhance qubit control.

I. INTRODUCTION

A. Quantum Dot Qubit Dynamics

Recent advancements in the utilization of hole spin states within strained germanium (Ge/SiGe) gate-defined quantum dots have significantly enhanced qubit operations. Germanium offers multiple benefits for these applications. A prominent advantage is the wide gap between the topmost valence bands, easing access to the primary hole states for spin encoding. Moreover, germanium exhibits a prolonged coherence time, crucial for stable qubit performance, and strong spin-orbit coupling in hole spins. This allows for all-electric qubit control by adjusting the spin-orbit Hamiltonian through electric gates, thus eliminating the need of micromagnets.

One critical advantage of germanium that is highly relevant to this study is illustrated through the Hamiltonian of a double quantum dot qubit, presented as follows:

$$\mathbf{H} = \begin{pmatrix} -J(\epsilon) & \Delta \\ \Delta & -\bar{E}_z \end{pmatrix} \tag{1}$$

In this representation, the Hamiltonian is defined in the $\{|S\rangle, |T_-\rangle\}$ basis. The diagonal terms, $J(\epsilon)$ and $\bar{E}_z = \bar{g}\mu_B B$, correspond to the exchange energy at detuning ϵ and the average Zeeman energy, respectively. The off-diagonal term, Δ, is given by:

$$\Delta = \left| \Delta_{\mathrm{SO}} \sin\left(\frac{\Omega}{2}\right) + g_\alpha \mu_B B \cos\left(\frac{\Omega}{2}\right) \right| \tag{2}$$

This term mixes the singlet and triplet states by incorporating the effects of the spin-orbit energy splitting (Δ_{SO}) and the g-tensor (g_α). The presence of the g-factor in the Hamiltonian significantly impacts the control of the quantum dot qubit, emphasizing the importance of detailed understanding of its distribution in the quantum dot device.

The state of the qubit can be manipulated by altering the detuning ϵ and the Zeeman splitting $\bar{E}_z$. When $J(\epsilon) \approx \bar{E}_z$, the Hamiltonian resembles the Pauli X matrix, effectuating a rotation around the x-axis on the Bloch sphere. As $J(\epsilon)$ approaches zero, which occurs at large detuning, the qubit rotates around an axis that is a linear combination of the x and z-axes. The proximity of the rotation axis to the z-axis increases as the ratio $\frac{\bar{E}_z}{\Delta}$ becomes larger. The rotation frequency of the qubit is given by the equation:

$$f = \frac{1}{h}\sqrt{(J - \bar{E}_z)^2 + (2\Delta)^2} \tag{3}$$

This formula quantifies the dynamics of the qubit's rotational behavior in terms of the tunable parameters J, $\bar{E}_z$, and Δ.

Practically, both the detuning and the Zeeman energy can be tuned by adjusting the gate voltages, which also allows for modulation of the average g-factor as the voltage reshapes the quantum dot. The quantum dot device in our laboratory is depicted in Figure 1. The barrier gates B_L and B_R are utilized to confine the quantum dot, while the middle gate is responsible for controlling the coupling between the two dots [1].

B. g-Factor Correction Due to Strain

The motion of an electron in a periodic potential $V(\mathbf{r})$ under a uniform magnetic field $\mathbf{B}$ can be captured by the Luttinger-Kohn Hamiltonian:

$$H = H_k + H_\epsilon + H_z + V(\mathbf{r})\mathbb{I} \tag{4}$$

where H_k is the kinetic Hamiltonian, H_ϵ represents the strain Hamiltonian, and H_z is the Zeeman Hamiltonian. The two topmost valence bands of Germanium are known as the HH and LH, corresponding to the z-component of electron angular momentum $J_z = \pm\frac{3}{2}$ and $J_z = \pm\frac{1}{2}$, respectively (see Figure 2) [2]. We take this set of angular momentum $J_z = \{\pm\frac{3}{2}, \pm\frac{1}{2}\}$ eigenstates as basis, then the kinetic and strain Hamiltonian take the same form

$$H_{k/\epsilon} = \begin{pmatrix} P+Q & -S & R & 0 \\ -S^\dagger & P-Q & 0 & R \\ R^\dagger & 0 & P-Q & S \\ 0 & R^\dagger & S^\dagger & P+Q \end{pmatrix} \tag{5}$$

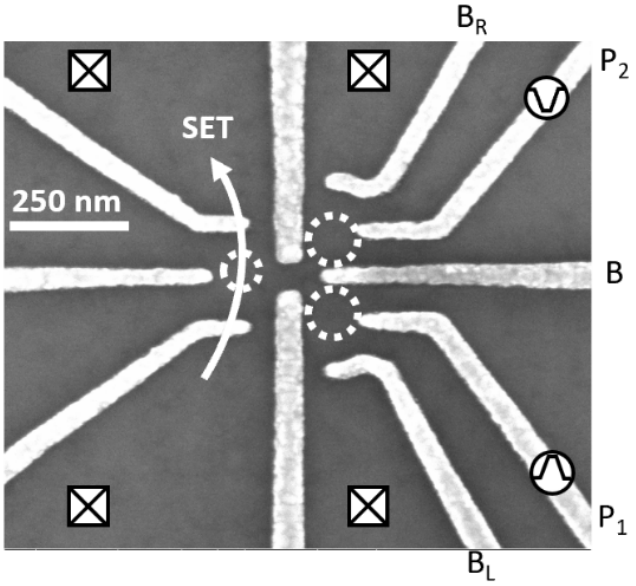

Figure 1. SEM image of lithographically defined gates identical to the geometry used in this study. B_L and B_R are confinement gates, P_1, P_2, and B are control gates, and FET is the readout gate.

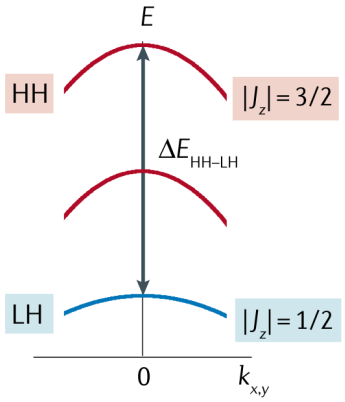

Figure 2. Sketch of band structure of germanium in a planar hetero-structure, corresponding to the geometry of our quantum dot device

For kinetic Hamiltonian, the P, Q, R, S variables are

$$\begin{aligned} P_k &= \frac{1}{2m_0}\gamma_1(p_x^2+p_y^2+p_z^2) \\ Q_k &= \frac{1}{2m_0}\gamma_2(p_x^2+p_y^2-2p_z^2) \\ R_k &= \frac{1}{2m_0}\sqrt{3}\left[-\gamma_2(p_x^2-p_y^2)+2i\gamma_3\{p_x,p_y\}\right] \\ S_k &= \frac{1}{2m_0}2\sqrt{3}\gamma_3\{p_x-ip_y,p_z\} \end{aligned} \tag{6}$$

where γ_1, γ_2, and γ_3 are the Luttinger parameters, determined entirely by the material properties. The terms p_x, p_y, and p_z represent the components of momentum, with the notation $\{A,B\} = AB + BA$ denoting the anti-commutator.

For the strain Hamiltonian, the P, Q, R, S variables are

$$\begin{aligned} P_\epsilon &= -a_v(\epsilon_{xx}+\epsilon_{yy}+\epsilon_{zz}) \\ Q_\epsilon &= -\frac{1}{2}b_v(\epsilon_{xx}+\epsilon_{yy}-2\epsilon_{zz}) \\ R_\epsilon &= \frac{\sqrt{3}}{2}b_v(\epsilon_{xx}-\epsilon_{yy})-id_v\epsilon_{xy} \\ S_\epsilon &= -d_v(\epsilon_{xz}-i\epsilon_{yz}) \end{aligned} \tag{7}$$

where $\epsilon_{\alpha\beta}$ represents components of the strain, a 3×3 tensor in three-dimensional space. The constants a_v, b_v, and d_v are the hydrostatic, uniaxial, and shear deformation potentials, respectively, describing how the band energy shifts with changes in the strain tensor. In Ge quantum dots, the dominant ground state is the HH state, while strain induces mixing between the LH and HH states, thereby altering the g-factor.

The effect of the deformation potentials can be more intuitively understood by considering the HH and LH energy in the decoupled band case, which is given by:

$$\begin{aligned} E_{HH}(\epsilon) &= E_{HH}(0)+a_v\mathrm{Tr}(\epsilon)+b_v(\epsilon_{zz}-\frac{1}{2}\epsilon_{xx}-\frac{1}{2}\epsilon_{yy}) \\ E_{LH}(\epsilon) &= E_{LH}(0)+a_v\mathrm{Tr}(\epsilon)-b_v(\epsilon_{zz}-\frac{1}{2}\epsilon_{xx}-\frac{1}{2}\epsilon_{yy}) \end{aligned} \tag{8}$$

As indicated by the equations, a_v shifts both the HH and LH bands while b_v splits these two bands. In the general coupled case, d_v also participates in splitting the bands.

The g-factor, like the strain, is also a 3×3 tensor. The corrections to its components due to strain are given by:

$$\begin{aligned} \delta g_{xx} = \delta g_{yy} &= \frac{6b_v\kappa}{\Delta_{\mathrm{LH}}}\left(\langle\epsilon_{yy}\rangle-\langle\epsilon_{xx}\rangle\right) \\ \delta g_{zy} &= -\frac{4\sqrt{3}kd_v}{\Delta_{\mathrm{LH}}}\langle\epsilon_{yz}\rangle \\ \delta g_{zx} &= -\frac{4\sqrt{3}kd_v}{\Delta_{\mathrm{LH}}}\langle\epsilon_{xz}\rangle \\ \delta g_{xy} = -\delta g_{yx} &= \frac{4\sqrt{3}d_v\kappa}{\Delta_{\mathrm{LH}}}\langle\epsilon_{xy}\rangle \end{aligned} \tag{9}$$

where κ is a material-specific parameter and Δ_{LH} is the energy splitting between LH and HH states [3].

C. Paper Outline

In this paper, we delve into the significance of the g-factor in qubit dynamics, focusing on how strain within quantum dot devices leads to modifications in the g-factor. We employ the FEM to simulate thermal contraction strain within a specific quantum dot device geometry as depicted in Figure 1, analyzing the resultant distribution of g-factor corrections. Section II.A introduces the fundamentals of linear elasticity theory, discussing the relationship between displacement vectors, stress tensors, and strain tensors. Following this, Section II.B addresses thermal elasticity,

exploring how differential thermal expansion coefficients across various materials in a heterogeneous device give rise to strain. This section includes the derivation of the linear thermal-elasticity equation and its weak form—the specific formulation we solve using FEM. In Section III, we detail our methodological approach, from constructing the mesh geometry and setting solver parameters for calculating temperature and displacement, to deriving strain from displacement measurements. This section also justifies our choice of using a weak coupling approach and lists all the parameters utilized in our simulations. Section IV culminates with the presentation of our findings, showcasing the distribution of g-factor corrections and their implications for enhancing control in quantum dot devices. This comprehensive study not only enriches the existing literature on thermal contraction strain-induced g-factor correction but also opens avenues for precise tuning of quantum dot characteristics in future research.

II. THEORY

A. Linear Elasticity Theory

1. The Strain Tensor

Strain is a measure that describes the extent to which a material is stretched or compressed. Focusing on a single point within the material, the deformation manifests as the displacement of that point, defined by the displacement vector:

$$u_i = x_i' - x_i \tag{10}$$

where x_i and x_i' are the locations before and after displacement, respectively. Consider two points initially separated by a small distance $dl = \sqrt{\sum_i x_i^2}$. If their displacement vectors differ by du, then after displacement, their separation becomes $dl' = \sqrt{\sum_i x_i'^2} = \sqrt{\sum_i (dx_i + du_i)^2}$. Since displacement depends on the original position in all three directions, we can write:

$$du_i = \sum_k \frac{\partial u_i}{\partial x_k} dx_k$$

Thus, we can express dl'^2 in terms of variables prior to displacement:

$$\begin{aligned} dl'^2 =& \sum_i \left(dx_i + \sum_k \frac{\partial u_i}{\partial x_k} dx_k \right)^2 \\ =& \sum_i dx_i^2 + 2 \sum_{i,k} \frac{\partial u_i}{\partial x_k} dx_k dx_i + \sum_{k,l} \frac{\partial u_i}{\partial x_k} \frac{\partial u_i}{\partial x_l} dx_k dx_l \end{aligned} \tag{11}$$

The sum expression of the second term is symmetric with respect to indices i and k. By switching indices i and l in the third term, equation (11) becomes:

$$\begin{aligned} dl'^2 =& dl^2 + \sum_{i,k} \left(\frac{\partial u_i}{\partial x_k} dx_k dx_i + \frac{\partial u_k}{\partial x_i} dx_i dx_k \right) \\ &+ \sum_{i,k} \frac{\partial u_l}{\partial x_k} \frac{\partial u_l}{\partial x_i} dx_k dx_i \\ =& dl^2 + \sum_{i,k} 2\epsilon_{ik} dx_i dx_k \end{aligned} \tag{12}$$

where the strain tensor is defined as:

$$\epsilon_{ik} = \frac{1}{2} \left(\frac{\partial u_i}{\partial x_k} + \frac{\partial u_k}{\partial x_i} + \frac{\partial u_l}{\partial x_i} \frac{\partial u_l}{\partial x_k} \right) \approx \frac{1}{2} \left(\frac{\partial u_i}{\partial x_k} + \frac{\partial u_k}{\partial x_i} \right) \tag{13}$$

This approximation assumes small strain, implying minimal displacement. It is possible to experience significant displacement even with minor internal deformation—for instance, a thin, long rod may display large end displacements even under minor strain. However, in a 3D body where no dimension is significantly smaller than the others, such displacement remains minimal. This scenario applies to our quantum dot device geometry; thus, we will use this approximated equation throughout the paper.

From equation (13), we observe that the strain tensor is symmetric and therefore diagonalizable at any point. Consequently, the expression for dl'^2 becomes decoupled in the directions of the three eigenvectors of the strain tensor:

$$dl'^2 = \sum_i (1 + 2\epsilon^{(i)}) dx_i^2 \tag{14}$$

Here, $\epsilon^{(i)}$ denotes the i^{th} eigenvalue, and the relative extension along the i^{th} axis is approximately $\epsilon^{(i)}$, given by $\sqrt{1 + 2\epsilon^{(i)}} - 1$. This leads to a change in volume expressed as:

$$dV' = dV \prod_i (\epsilon^{(i)} + 1) \approx dV (1 + \sum_i \epsilon^{(i)}) \tag{15}$$

where higher order terms are neglected in the final approximation. Since the sum of the eigenvalues of a matrix equals its trace [4], we find that the trace of the strain tensor dictates the volume change after deformation, as shown by:

$$\frac{dV' - dV}{dV} = \mathrm{Tr}(\epsilon) = \sum_i \epsilon_{ii} \tag{16}$$

For a traceless strain tensor, the volume remains invariant during deformation (although the shape may change), which we term pure shear. Conversely, if the strain tensor equals a constant times the identity matrix, the shape remains invariant during deformation (while the volume may change), termed hydrostatic deformation. We can always decompose the strain tensor into its pure shear and hydrostatic components, an expression crucial for later discussions:

$$\epsilon_{ik} = \left(\epsilon_{ik} - \frac{1}{3} \delta_{ik} \mathrm{Tr}(\epsilon) \right) + \frac{1}{3} \delta_{ik} \mathrm{Tr}(\epsilon) \tag{17}$$

2. The Stress Tensor

When a body is deformed from equilibrium, an internal force emerges that tends to restore it to its original state. This force is linked to internal stress. Before we delve into the definition of the stress tensor, let's first examine this force. Consider the total force experienced by a volume dV within the body, which can be expressed as $\mathbf{F}dV$, where $\mathbf{F}$ is the force per unit volume, represented as a vector. According to Newton's third law, internal forces within a material cancel each other out, meaning the total force experienced by the volume must equal the total external force acting upon it. This external force acts through the surface of the volume, necessitating that the volume integral $\int \mathbf{F}dV$ be expressible as a surface integral. According to the divergence theorem, the volume integral of a vector field is equivalent to a surface integral if the vector field is the divergence of some tensor field. Applying this principle to each component of $\mathbf{F}$, we conclude that $\mathbf{F}$ must be the divergence of a rank two tensor, typically called the stress tensor, described by the relationship:

$$F_i = \sum_k \frac{\partial \sigma_{ik}}{\partial x_k} \tag{18}$$

Consequently, the total force can be expressed as:

$$\int \mathbf{F}dV = \int \sum_k \frac{\partial \sigma_{ik}}{\partial x_k} dV = \int \sum_k \sigma_{ik} df_k \tag{19}$$

This formula gives the interpretation of $\sum_k \sigma_{ik} df_k$ as the i^{th} component of force acting on a surface element $d\mathbf{f}$. Here, σ_{ik} represents the i^{th} component of force per area acting on the k^{th} component of the surface, which is normal to direction k. For instance, σ_{xx} is the x-component of the force per area vector acting on a surface perpendicular to the x-axis (a normal force), while σ_{xy} is the y-component of the force acting on a surface perpendicular to the x-axis (a tangential force) [5].

B. Thermodynamic of Elasticity

1. Work Done by Stress

We previously derived the relationship between force per unit volume and stress in equation (18). To calculate the work done by stress, we multiply the force by a displacement δu:

$$\begin{aligned} W &= \int_\Omega \sum_{k,i} \frac{\partial \sigma_{ik}}{\partial x_k} \delta u_i dV \\ &= \oint_{\partial\Omega} \sum_{k,i} \sigma_{ik} \delta u_i df_k - \int_\Omega \sum_{k,i} \sigma_{ik} \frac{\partial \delta u_i}{\partial x_k} dV \end{aligned} \tag{20}$$

The second equality is derived using integration by parts with respect to x_k. We can freely choose the domain of integration Ω in equation (20). Assuming the object is not deformed at infinity, we may let Ω encompass the entire space, causing the surface integral to vanish. Thus,

$$\begin{aligned} W &= -\int_\Omega \sum_{k,i} \sigma_{ik} \frac{\partial \delta u_i}{\partial x_k} dV \\ &= -\frac{1}{2} \int_\Omega \sum_{k,i} \sigma_{ik} \left(\frac{\partial \delta u_i}{\partial x_k} + \frac{\partial \delta u_k}{\partial x_i} \right) dV \\ &= -\frac{1}{2} \int_\Omega \sum_{k,i} \sigma_{ik} \delta \left(\frac{\partial u_i}{\partial x_k} + \frac{\partial u_k}{\partial x_i} \right) dV \\ &= \int_\Omega \sum_{k,i} \sigma_{ik} \delta \epsilon_{ik} dV = \int_\Omega \sigma(\mathbf{u}) : \delta\epsilon(\mathbf{u}) dV \end{aligned} \tag{21}$$

This yields the expression of work in terms of the double contraction of the stress tensor by the change in the strain tensor. This work must be balanced by the external work done on the surface of the object. Assuming the force per unit area of the external force is $\mathbf{T}$, we obtain the following equation:

$$\forall \mathbf{v} \in V: \quad \int_\Omega \sigma(\mathbf{u}) : \epsilon(\mathbf{v}) d\Omega = \int_{\partial\Omega} \mathbf{T} \cdot \mathbf{v} dS \tag{22}$$

This is the equation that we will solve using FEM in this study, where $\mathbf{v}$ is the test function and V is the function space which contains both the test function $\mathbf{v}$ and the solution $\mathbf{u}$.

2. Free Energy of Deformation

An infinitesimal change in internal energy dU is equal to the heat transferred to the system minus the work done by the system. Using equation (21), we have:

$$dU = TdS + \sum_{i,k} \sigma_{ik} d\epsilon_{ik} \tag{23}$$

The free energy $\mathcal{F}$ is related to the internal energy by $\mathcal{F} = U - TS$. This gives us its total differential:

$$\begin{aligned} d\mathcal{F} &= dU - TdS - SdT \\ &= -SdT + \sum_{i,k} \sigma_{ik} d\epsilon_{ik} \end{aligned} \tag{24}$$

Then, under constant temperature, we derive an important differential relation that links the stress tensor to the strain tensor:

$$\sigma_{ik} = \left(\frac{\partial \mathcal{F}}{\partial \epsilon_{ik}} \right)_T \tag{25}$$

3. Expansion of Free Energy

We aim to expand the free energy up to the second order of the strain tensor, represented as $\mathcal{F} = \mathcal{F}_0 + \mathcal{F}_1 + \mathcal{F}_2$. From equation (25), the first order derivative of free energy with respect to the strain corresponds to the stress. In the undeformed state, where the stress is zero, the first order term in the expansion does not contribute. The expansion includes two independent second order

terms: the squared sum of the diagonal entries and the squared sum of all entries, expressed as:

$$\mathcal{F} = \mathcal{F}_0 + \frac{1}{2}\lambda \sum_i \epsilon_{ii}^2 + \mu \sum_{i,k} \epsilon_{ik}^2 \tag{26}$$

where λ and μ are known as the Lamé parameters. We can separate the diagonal and off-diagonal parts in the second term using equation (17):

$$\mathcal{F} = \mathcal{F}_0 + \mu \sum_{i,k} \left(\epsilon_{ik} - \frac{1}{3}\delta_{ik}\epsilon_{ll}\right)^2 + \frac{1}{2}K \sum_l \epsilon_{ll}^2 \tag{27}$$

where K is called the bulk modulus and is related to the Lamé parameters by $K = \lambda + \frac{2}{3}\mu$.

4. *Deformation Due to Change of Temperature*

Suppose the undeformed temperature of a body is T_0. At a different temperature $T \neq T_0$, the body will deform, leading to the introduction of a first-order term in the expansion of free energy. This term must be linear and scalar, and the only suitable candidate is the trace of the strain tensor. For small deformations, we can assume that the coefficient of this linear term linearly depends on the temperature. Since this first-order term vanishes at $T = T_0$, we define this coefficient as $-K\alpha(T - T_0)$, where α is the thermal expansion coefficient. Consequently, the free energy can be expressed as:

$$\begin{aligned}\mathcal{F} =& \mathcal{F}_0 - K\alpha(T - T_0)\,\mathrm{Tr}(\epsilon) \\ &+ \mu \sum_{i,k} \left(\epsilon_{ik} - \frac{1}{3}\delta_{ik}\epsilon_{ll}\right)^2 + \frac{1}{2}K \sum_l \epsilon_{ll}^2\end{aligned} \tag{28}$$

To solve equation (22), we describe the stress tensor as a function of the strain tensor, utilizing the differential relationship from equation (25):

$$\begin{aligned}\sigma_{ik} =& -K\alpha(T - T_0)\delta_{ik} \\ &+ K \sum_l \delta_{ik}\epsilon_{ll} + 2\mu \left(\epsilon_{ik} - \frac{1}{3}\delta_{ik} \sum_l \epsilon_{ll}\right)\end{aligned} \tag{29}$$

Notice that the sum symbol over i, k disappears when taking the differential. When the differential of $\mathcal{F}$ involves a specific entry of the strain tensor, terms in the sum with different indices are independent of that entry and consequently vanish [5]. For convenience of FEM analysis, we may alternatively express this as:

$$\sigma = \lambda\,\mathrm{Tr}(\epsilon)\mathbf{I} + 2\mu\epsilon - \alpha(3\lambda + 2\mu)(T - T_0)\mathbf{I} \tag{30}$$

Substituting this expression into equation (22), we derive the final form of the equation to be solved in this study [6].

III. METHOD

A. Geometry for Simulation

Note that here are two types of geometric entities in Gmsh, the elementary entities are those created for the convenience of building geometry, while physical entities are groups of elementary entities created to make the interpretation of them in coding easier. For example, if we want to define a boundary condition that the displacement vector on the outmost surfaces of the geometry are 0, there might be many surfaces that constitute the outmost facet of the device. While in Gmsh, we can group these surfaces into a physical group, which can be read directly by FEniCS as one entity. We defined physical volume such that each physical volume corresponds to a material, since we need to define material specific parameters to each volume in FEniCS. We defined two physical surfaces, one corresponds to the bottom and side surface of the device, while the other is the top surface.

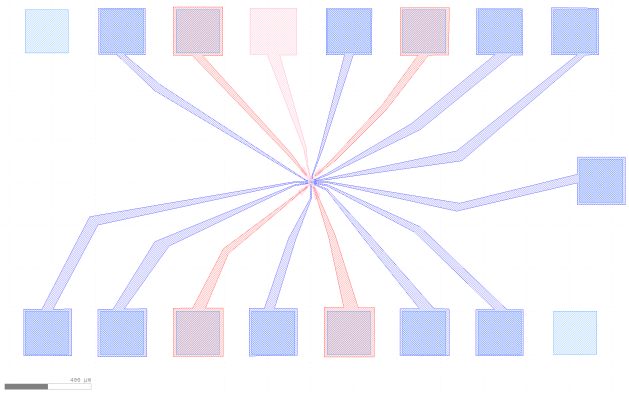

Figure 3. View of the entire device in Klayout, which has length scale about 10^2 micrometers, while the region we selected for simulation has length scale around 10^0 micrometer

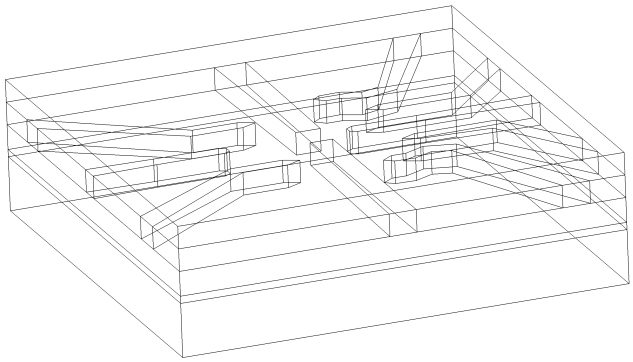

Figure 4. View of the simulation geometry in Gmsh, detailing the layer structure of the device. From bottom to top: a 120nm thick $Ge_{0.8}Si_{0.2}$ layer, a 16nm thick Ge layer, a 55nm thick $Ge_{0.8}Si_{0.2}$ layer, a 50nm thick Al gate layer, and a 50nm thick Al_2O_3 cap layer. Areas not occupied by gates within the gate layer are also filled with Al_2O_3.

B. Meshing

To solve the thermal elasticity equation on our geometry using the Finite Element Method (FEM), we need to partition it into mesh grids. Each grid consists of vertices, facets, and a cell. The discretized equation

is solved at each vertex using boundary conditions defined on the facets, and numerical values are assigned to the cell based on the type of element used. For instance, in a first-order element, the solution within the cell is computed linearly from the solutions at the vertices. Gmsh allows for the customization of mesh grid sizes in different regions. There are two crucial considerations when defining the mesh: the accuracy of the solution and the computational time. Increasing the number of mesh grids or the order of the cell element generally enhances accuracy but also demands more computation time and resources. To balance these competing requirements, our strategy involves reducing the number of mesh grids in regions where the solution may be more uniform or in areas less critical to our study. Conversely, we employ an extremely refined mesh in the Germanium layer, where we anticipate complex strain distributions based on previous literature [3, 7] and because it is the location of the quantum dot occurrence, crucial for calculating g-factor corrections. For details of the mesh definition, see Figures 5 and 6.

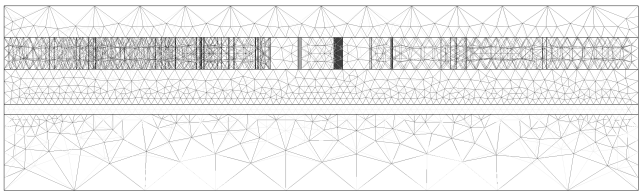

Figure 5. Side view of the mesh used for simulation, illustrating how we controlled mesh grid density using the transfinite mesh feature of Gmsh. Each edge of the bottom surface features 10 vertices, each edge of the top surface has 15 vertices, and each edge in the Germanium layer boasts 100 nodes. The mesh is intentionally denser in the Germanium layer and within the Aluminum gates, as these areas significantly influence the strain in the Germanium layer.

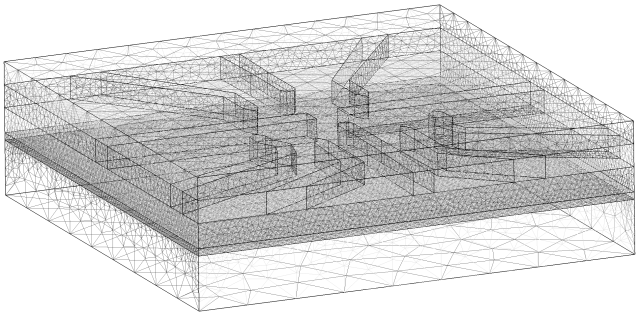

Figure 6. 3D view of the mesh

C. The Temperature Problem

1. Weak Coupling

Equation (30) indicates that the PDEs we need to solve are dependent on the temperature T, requiring us to specify the temperatures considered for solving Equations (30) and (22). We know that our quantum dot device is assembled at room temperature (approximately 300K) and operates at cryogenic temperatures (around 20K). Therefore, we adopt these two temperatures as the undeformed temperature T_0 and the current operating temperature T, respectively.

Physically, temperature changes induce strain due to differential thermal expansion coefficients of the materials used, while strain can also affect the temperature distribution. This interaction suggests that the thermal and mechanical issues are coupled. However, in this study, we do not consider the full coupling. We derived Equation (30) using the differential relation (25), which assumes constant temperature. Thus, our study operates under the 'weak coupling assumption,' implying that temperature changes due to strain are negligible.

Under this assumption, we first solve the temperature problem, which involves addressing the thermal conduction condition under equilibrium conditions $\nabla \cdot (k\nabla T) = 0$, implying zero local flux density everywhere. Our boundary condition for the temperature problem sets 20K on all outermost surfaces, leading us to anticipate a uniform temperature distribution of 20K throughout the device. Given this uniformity, we assume a consistent thermal conduction coefficient k of 1 for all materials involved. Should there be a need to account for temperature gradients, such as different temperatures at the top and bottom of the device, it would be necessary to assign distinct k values for different materials.

2. Solver Settings for Temperature

We defined the temperature as an element of a first-order Continuous Galerkin (CG) function space. 'First-order' indicates that the solution within each mesh cell is approximated linearly. 'CG' signifies that the mesh element belongs to the standard Lagrange family, requiring continuity across the boundaries of each cell [8]. For a 3D problem, which is typically computationally intensive, optimizing mesh design is crucial. Additionally, selecting an efficient linear solver and preconditioner pair can significantly enhance computational efficiency. In this study, we selected the 'gmres' and 'hypre-amg' pair.

GMRES (Generalized Minimal Residual Method) is an iterative solver ideal for the numerical solution of systems of linear equations, particularly those derived from sparse matrices. It excels in solving non-symmetric and ill-conditioned systems, often encountered in complex PDEs modeled through finite element analysis. This method aims to minimize the Euclidean norm of the residual vector across a Krylov subspace, expanding this subspace incrementally until the solution converges or a set number of iterations is completed.

Hypre is a library of high-performance preconditioners and solvers, notable for its implementation of Algebraic

Multigrid (AMG) methods. These methods are effective preconditioners for large-scale linear systems. AMG constructs a hierarchy of coarser grids that aids in accelerating the convergence of iterative solvers like GMRES by approximately solving the system on a coarser grid that encapsulates the problem's large-scale dynamics before refining the solution on finer grids. This preconditioner is particularly beneficial for problems like ours, which involve higher dimensions and detailed meshing [9].

3. *Temperature Solution*

Using the function space and solver defined in the previous subsection, we successfully resolved the thermal equilibrium problem. The resulting temperature difference (room temperature minus the current temperature) is illustrated in Figure 7.

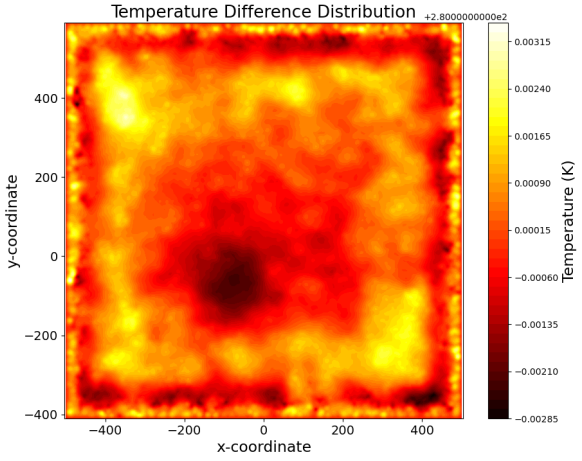

Figure 7. Temperature distribution captured at the plane parallel to the xy-plane at $z = -60$ nm, located in the center of the Germanium layer. This visualization shows the spatial temperature variations within the device.

From the figure, it is apparent that the temperature difference across the entire device maintains a nearly uniform level of 280K, with slight variations on the order of 10^{-3} K. These minor discrepancies can be attributed to the intrinsic characteristics of the numerical algorithm used for the simulation. The overall uniform temperature difference of 280K aligns with our simulation goals.

D. The Mechanical Problem

1. *Material Dependent Parameters*

In this problem, we need to define three parameters as stipulated by equation (30): the two Lamé parameters, λ and μ, and the thermal expansion coefficient α for four different materials—Ge, Al, $Ge_{0.8}Si_{0.2}$, and Al_2O_3. The Lamé parameters are relatively straightforward as they are not temperature-dependent. Table I summarizes the Lamé parameters for each material used in this study [3].

Parameter\Material	Ge	$Ge_{0.8}Si_{0.2}$	Al_2O_3	Al
λ	49.0	52.2	63.3	61.37
μ	68.8	71.1	68.5	30.9

Table I. Lamé parameters that we used for all the materials involved in this study

The situation for the thermal expansion coefficient is more nuanced because it is temperature-dependent, and this dependence varies across different materials. As we are solving the problem at 20K, we need the coefficients at this temperature, but available information is limited. For some materials, alternative approaches were necessary. We obtained the data for Ge and Al directly. For $Ge_{0.8}Si_{0.2}$, we accessed a graph of the thermal expansion coefficient versus temperature but lacked detailed numerical data, leading us to estimate its value at 20K visually. For Al_2O_3, the lowest temperature data available was at 100K, which we used in this study. We recognize that the thermal expansion coefficient for Al_2O_3 decreases significantly at lower temperatures, potentially leading to inaccuracies due to the difference between 100K and 20K coefficients. However, 100K is the closest data point we could obtain, and once more data becomes available, updating the value in our analysis framework will be straightforward. The thermal expansion coefficients utilized are summarized in Table II.

Parameter \Material	Ge	$Ge_{0.8}Si_{0.2}$	Al_2O_3	Al
$\alpha(\times 10^{-6})$	2.4 [11]	52.2 [12]	63.3 [13]	61.37 [14]

Table II. Thermal expansion coefficients parameters that we used for all the materials involved in this study

2. *Displacement Solution*

The displacement, which influences both the strain and stress tensors, is the sole variable in equation (22). Therefore, in solving this equation, we primarily focused on determining the displacement. Similar to the temperature analysis, we utilized the 'gmres' and 'hypre-amg' solver and preconditioner combination. We also explored different solver and preconditioner options. Our results indicate that GMRES provides the same solution quality as the Conjugate Gradient Method (CG), which was employed in the study by Abadillo-Uriel et al. [3]. However, the AMG preconditioner significantly enhanced computational efficiency, reducing computation time from approximately 8 minutes to 1 minute.

With the boundary condition that displacement is zero at all outermost surfaces, and by incorporating the previously solved temperature difference into

equation (30), we successfully obtained the solution for displacement. Subsequently, we extracted components of the displacement for visualization purposes. Figure 8 showcases the x-component of displacement, which distinctly mirrors the symmetry of the gates in our device geometry.

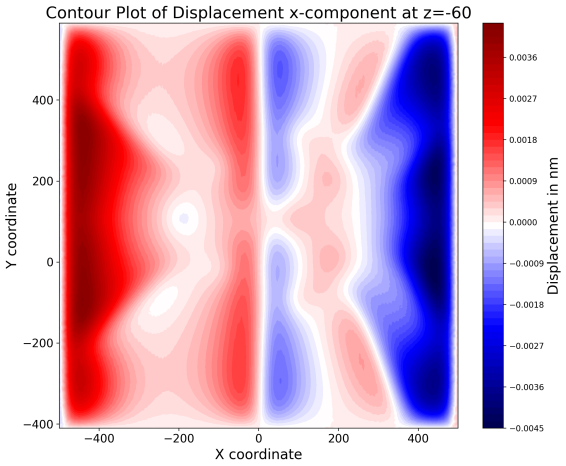

Figure 8. X-component of the displacement vector captured at horizontal surface with $z = -60$

3. *Strain Solution*

In equation (13), if we consider only the second term, we can see that the strain tensor is essentially the gradient of the displacement vector. Given that the first term is symmetric to the second term, we can also derive the strain tensor components from the gradient of the displacement vector. We computed the following quantities related to the components of the strain tensor: $\epsilon_{yy} - \epsilon_{xx}$, ϵ_{xz}, ϵ_{yz}, and ϵ_{xy}. The results are shown in Figure 9, with all plots obtained from the horizontal surface at $z = -60$.

We observed that the strain on the edge of the device is significantly higher than in the central region, which is our area of interest. Plotting all values without filtering would result in contour plots that fail to capture the distribution shape in the central area effectively. Therefore, we filtered out portions of the data representing the highest and lowest values, with the exact portion varying depending on the quantity being plotted. We aimed to exclude data from regions outside our area of interest while ensuring that the filtered data appropriately scales to capture the distribution within the central area. From the figure, we can observe that the magnitude of strain is at about 10^{-4} which aligns with the result in [3].

4. *g-Factor Correction Parameters*

As indicated in equation (9), g-factor corrections are related to strain by a factor. The relevant parameters b_μ, d_μ, κ, and Δ_{LH} are also material dependent, however, since we are only interested in the quantum dot region which is entirely in the Germanium layer, we only need data for Germanium. The data are summarized in table III [10].

Material\Parameter	b_v (eV)	d_v (eV)	κ	Δ_{LH} (eV)
Ge	-2.160	-6.060	3.410	7.1×10^{-2}

Table III. g-factor correction parameters that we used for Germanium

IV. RESULT

Based on Equation (9) and our parameter definitions in Section III.D.4, we evaluated the corrections to the g-factor, as illustrated in Figure 10. From the plots, it is evident that the in-plane g-factor corrections, g_{xx} and g_{xy}, are on the order of $10^{-2}\mathrm{V}^{-1}$, whereas the out-of-plane corrections, g_{zx} and g_{zy}, are approximately $10^{-1}\mathrm{V}^{-1}$. This observation aligns with the findings reported in [3]. Given that the g-factor of a free electron is 2, our results indicate that strain within the quantum dot device significantly alters the g-factor, particularly for the out-of-plane components. Moreover, our device exhibits approximate symmetry with respect to the horizontal axis through the middle of the xy-plane, which is mirrored in the symmetry of the g-factor correction distribution. Unlike our study, the device examined in [3] also demonstrates symmetry when reflected across the vertical axis, resulting in g-factor distributions symmetric about both axes. This consistency in symmetry between the device geometry and g-factor correction observed in both studies lends credibility to our results.

V. CONCLUSION

In this study, we simulated the distribution of corrections to the g-factor in our quantum dot device. Initially, we elucidated the significance of the g-factor in controlling qubit devices by explicitly detailing its contribution to terms in the double quantum dot qubit Hamiltonian. We then introduced the equation linking the strain tensor to g-factor corrections and derived the equation describing strain due to thermal expansion or contraction. This was formulated in the weak form suitable for solving using the FEM. We discussed the mesh geometry, linear solvers, and parameters used in this study, explaining the rationale behind our critical choices. Our results reveal that thermal contraction significantly influences the g-factor, with out-of-plane g-factor component corrections on the order of 10^{-1} of the free electron's g-factor and in-plane corrections on the order of 10^{-2}.

Our research enriches the existing literature by confirming several key aspects of thermal contraction-induced g-factor correction in quantum dot devices with a novel device geometry. By mapping

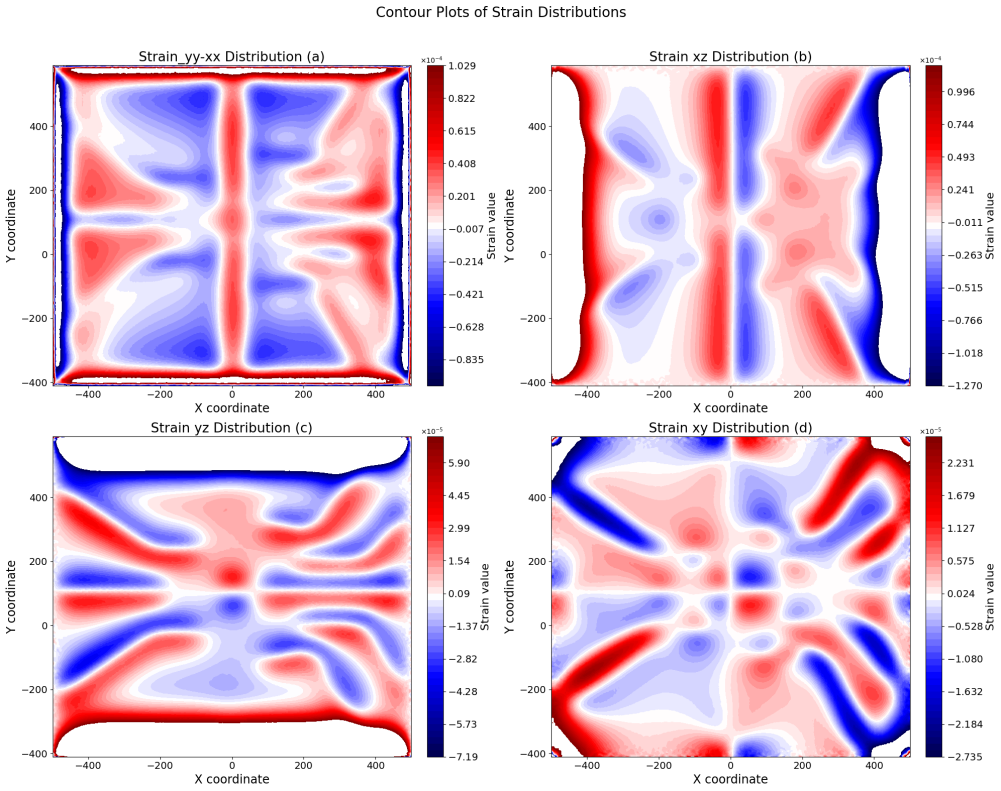

Figure 9. (a) Distribution of $\epsilon_{yy} - \epsilon_{xx}$, with top and bottom 3% of data removed. (b) Distribution of ϵ_{xz}, with top and bottom 8% of data removed. (c) Distribution of ϵ_{yz} with top and bottom 10% data filtered. (d) Distribution of ϵ_{xy}, with top and bottom 1% of data filtered.

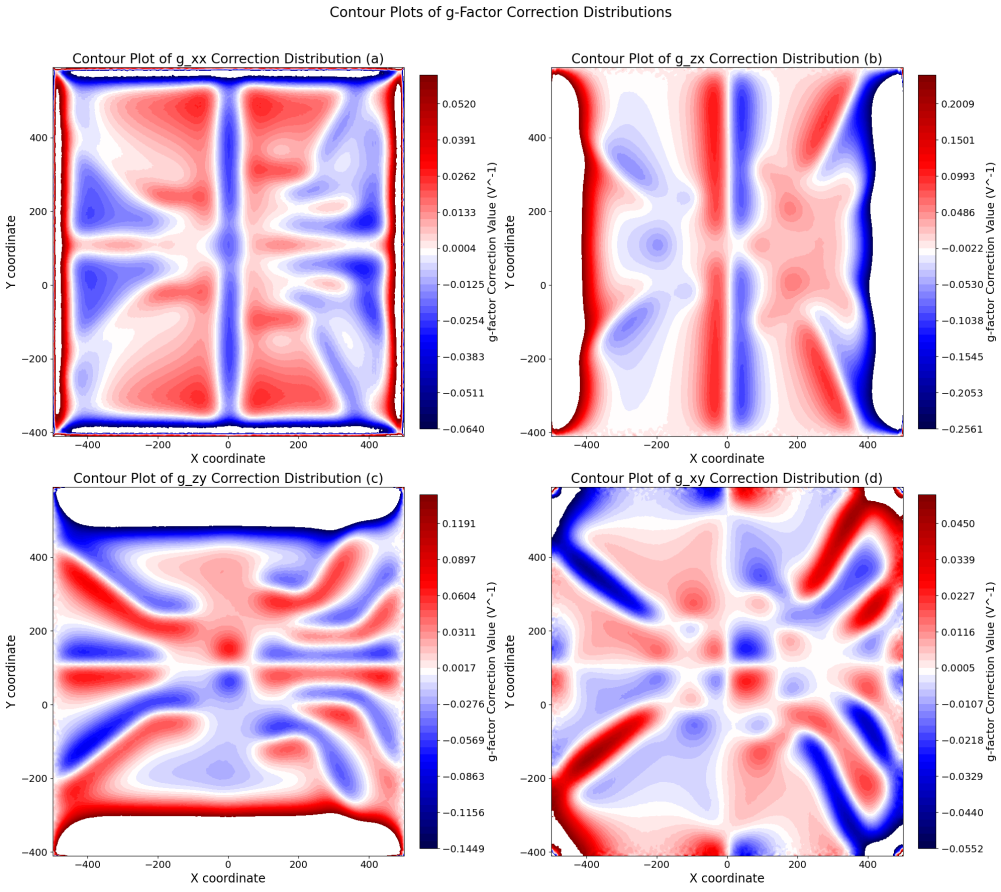

Figure 10. Distribution of g-factor correction components. The data filtering approach used here is consistent with that employed in the strain analyses.

the distribution of corrected g-factor, our study lays the groundwork for future research aimed at precisely tuning the average g-factor within the quantum dot region to enhance qubit control.

However, this study is not without potential shortcomings that future research could address. Firstly, the thermal expansion parameters used for Al_2O_3 at 20K are not entirely reliable, and secondly, the mesh configuration could be further optimized. Currently, we have only three layers of mesh in the germanium layer, including its top and bottom surfaces. Increasing the number of mesh layers could facilitate a more detailed study of how the g-factor correction distribution varies with the depth of the germanium layer.

[1] Rooney, John, Zhentao Luo, Lucas E. A. Stehouwer, Giordano Scappucci, Menno Veldhorst, and Hong-Wen Jiang. "Gate Modulation of the Hole Singlet-Triplet Qubit Frequency in Germanium." arXiv, November 16, 2023. http://arxiv.org/abs/2311.10188

[2] Scappucci, Giordano, Christoph Kloeffel, Floris A. Zwanenburg, Daniel Loss, Maksym Myronov, Jian-Jun Zhang, Silvano De Franceschi, Georgios Katsaros, and Menno Veldhorst. "The Germanium Quantum Information Route." Nature Reviews Materials 6, no. 10 (December 21, 2020): 926–43. https://doi.org/10.1038/s41578-020-00262-z

[3] Abadillo-Uriel, José Carlos, Esteban A. Rodríguez-Mena, Biel Martinez, and Yann-Michel Niquet. "Hole-Spin Driving by Strain-Induced Spin-Orbit Interactions." Physical Review Letters 131, no. 9 (September 1, 2023): 097002. https://doi.org/10.1103/PhysRevLett.131.097002

[4] Taboga, Marco (2021). "Properties of eigenvalues and eigenvectors", Lectures on matrix algebra. https://www.statlect.com/matrix-algebra/properties-of-eigenvalues-and-eigenvectors

[5] Landau, L. D., Lifshitz, E. M., Kosevich, A. M., Lifshitz, E., & Pitaevskii, L. P. (1986). Theory of elasticity: Volume 7. Elsevier.

[6] Axisymmetric formulation for elastic structures of revolution — Numerical tours of continuum mechanics using FEniCS master documentation. (n.d.). https://comet-fenics.readthedocs.io/en/latest/demo/elasticity/axisymmetric_elasticity.html

[7] Corley-Wiciak, Cedric, Carsten Richter, Marvin H. Zoellner, Ignatii Zaitsev, Costanza L. Manganelli, Edoardo Zatterin, Tobias U. Schülli, et al. "Nanoscale Mapping of the 3D Strain Tensor in a Germanium Quantum Well Hosting a Functional Spin Qubit Device." ACS Applied Materials & Interfaces 15, no. 2 (January 18, 2023): 3119–30. https://doi.org/10.1021/acsami.2c17395

[8] FunctionSpace — FENICS Project. (n.d.). https://fenicsproject.org/olddocs/dolfin/1.4.0/python/programmers-reference/functions/functionspace/FunctionSpace.html

[9] Solving PDEs in Python - The FENICS Tutorial Volume I. (n.d.). https://fenicsproject.org/pub/tutorial/html/._ftut1017.html

[10] Abadillo-Uriel, Jose Carlos, Esteban A Rodrıguez-Mena, Biel Martinez, and Yann-Michel Niquet. "Supplementary Material for 'Hole Spin Driving by Strain-Induced Spin-Orbit Interactions,'" n.d.

[11] Sparks, P. W., and C. A. Swenson. "Thermal Expansions from 2 to 40°K of Ge, Si, and Four III-V Compounds." Physical Review 163, no. 3 (November 15, 1967): 779–90. https://doi.org/10.1103/PhysRev.163.779.

[12] Levinshtein, M. E., Rumyantsev, S. L., & Shur, M. S. (2001). Properties of advanced semiconductor materials: GaN, AIN, InN, BN, SiC, SiGe. John Wiley & Sons.

[13] Schauer, Alois. "Thermal Expansion, Grueneisen Parameter, and Temperature Dependence of Lattice Vibration Frequencies of Aluminum Oxide." Canadian Journal of Physics 43, no. 4 (April 1965): 523–31. https://doi.org/10.1139/p65-049

[14] Clark, A.F. "Low Temperature Thermal Expansion of Some Metallic Alloys." Cryogenics 8, no. 5 (October 1968): 282–89. https://doi.org/10.1016/S0011-2275(68)80003-7